Mineral Mapping Mauna Kea and Mauna Loa Shield Volcanos on Hawaii Using AVIRIS Data and the USGS Tetracorder Spectral Identification System: Lessons Applicable to the Search for Relict Martian Hydrothermal Systems

Gregg A. Swayze,[1] Roger N. Clark,[1] Stephen J. Sutley,[1] Carol A. Gent,[1] Barnaby W. Rockwell,[1] Diana L. Blaney,[2] James L. Post,[3] and Brian P. Farm[4]

INTRODUCTION

The Hawaiian AVIRIS campaign conducted during the spring of 2000 provided an opportunity to collect hyperspectral data over a unique geologic environment on the sides of two of the Earth's largest shield volcanos. High altitude AVIRIS data were collected on April 14, 2000 along a 75 km NE traverse passing over the summits of Mauna Kea (4205 m) and Mauna Loa (4064 m) encompassing the saddle (1940 m) between them. This traverse covers diverse climatic and ecological zones extending from tropical coastal forests to alpine tundra over an elevation range of 3200 m. The summits of both volcanos are among the highest and driest readily accessible areas in the world with the summit of Mauna Kea chosen as the site for the largest collection of telescopic observatories in the world. In the cool-dry atmosphere atop these shield volcanos, rocks are nearly devoid of macroscopic life and chemical weathering is relatively low. These extreme climatic conditions and extensive basalt outcrops combine to form one of the best terrestrial analogues to the Martian shield volcanos. Several studies have suggested that certain palagonitic soils from Mauna Kea are good spectral analogues of Martian surface materials (Singer et al., 1979, Singer, 1982; Evans and Adams, 1979, 1980; Allen et al., 1981, 1982). Other studies suggest that hydrothermal systems may have been sanctuaries for ancient life on Mars (Walter et al., 1993; Farmer and DeMarais, 1994; Wade et al., 1999). Examples of relict hydrothermal systems exist at the summits of both Mauna Kea and Mauna Loa, and these areas were measured by AVIRIS as terrestrial analogues of the mineral associations and spatial extent of hydrothermal systems developed in mafic volcanic rocks.

VOLCANIC HISTORY OF THE BIG ISLAND

There are five distinct volcanos that grew and merged to form the Big Island of Hawaii. The loci of volcanism (Fig. 1) has shifted progressively southeastward over time reflecting the NW motion of the Pacific plate over the Hawaiian hot spot (Clague and Dalrymple, 1987). The most intense subaerial volcanic activity is now centered at the two southernmost volcanos, Mauna Loa and Kilauea. The youngest and smallest volcano in the Hawaiian chain is Loihi which is growing beneath the sea 30 km SE of the Big Island (Wolfe and Morris, 1996 and references therein). Ideally a Hawaiian shield volcano goes through four stages during it life: preshield, shield, postshield, and rejuvenation (Clague and Dalrymple, 1987, 1989). Accordingly, the preshield stage involves initial eruption of alkalic basalt, followed by the shield building stage eruption of tholeiitic basalts (low in alkalis), which eventually gives way to the postshield stage eruption of more SiO_2-rich alkali hawaiite lavas. The rejuvenated stage involves the eruption of SiO_2-poor lava after a few million years

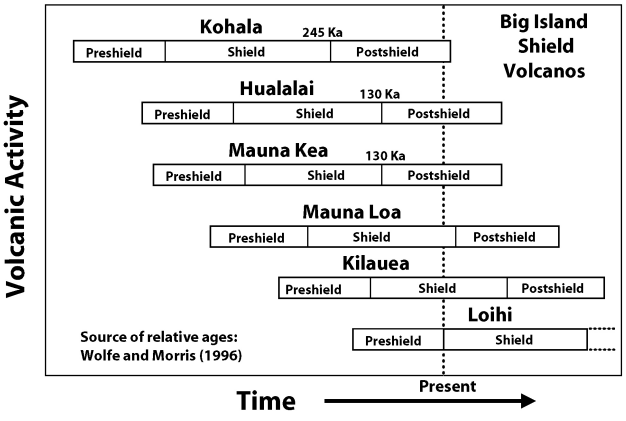

Figure 1. Growth stages of the Big Island shield volcanos.

[1]U.S. Geological Survey, MS964 Box 25046 DFC, Denver, Colorado 80225; gswayze@speclab.cr.usgs.gov
[2]Jet Propulsion Laboratory, 4800 Oak Grove Drive, Pasadena, California 91109
[3]Vector Engineering, Inc., 12438 Loma Rica Drive, Suite C, Grass Valley, California 95945
[4]Previously at the U.S. Geological Survey, Kilauea Volcanic Observatory, Hawaii

of quiescence, but no volcanos on the Big Island have reached this stage. Loihi is thought to be in transition from the preshield stage to the shield stage (Moore et al., 1982). Mauna Loa and Kilauea are in the shield building stage, which produces 95 to 98% of a volcano's volume (Wolfe and Morris, 1996) and typically lasts for about 500,000 years (Moore and Clague, 1992). Kohala, Hualalai, and Mauna Kea, being the oldest, are in the postshield stage and are capped by alkalic lavas. Shield volcanos grow from lava erupted at the summit of the volcano and from vents aligned along rift zones extending out from the summit, forming mountains elongated parallel to the rift zones (Wolfe et al., 1997). The Big Island has grown by addition of lavas to its SE flank and by seaward displacements along its active NE-trending rift zones. Mauna Loa has a fault-bounded caldera approximately 5 km in diameter (Fig. 2) which is a relatively recent feature only active for several centuries (Wolfe and Morris, 1996). Postshield eruptions transform broad, smoothly sloping shields into steeper, more irregularly-shaped edifices, by addition of more viscous lavas (Wolfe et al., 1997). The summit of Mauna Kea has numerous scoria cinder cones formed from the explosive eruption of more viscous and volatile-rich alkalic lavas typical of postshield volcanism.

Figure 2. View of Mokuaweoweo Caldera (looking SW) on the summit of Mauna Loa. Argillic alteration possibly produced by a small relict hydrothermal system is visible as a bleached area along the SW wall of the caldera.

IMAGING SPECTROSCOPY

Solar radiance, atmospheric absorptions, and scattering were removed from the AVIRIS data using the ATREM program (Gao et al., 1993). Artifacts from the ATREM processing were then removed by first subtracting a path radiance correction from the data and then multiplying by correction factors derived from field spectra of a ground calibration site using the method of Clark et al. (this volume). Because we were most interested in the geologic materials exposed near the summits of both volcanos, a calibration site at high elevation was chosen to minimize the effects of imperfect removal of atmospheric CO_2. Landsat 7 ETM+ data were analyzed and a spectrally bland, non-hydrothermally altered area was chosen as a field calibration site. Field spectral measurements of a relatively flat post-glacial alluvial fan deposit located near the summit of Mauna Kea at 4000 m and 0.45 km SE of the Puu Poliahu Cinder Cone were used to derive a multiplicative correction (Figs. 3 and 4). A total of 233 spectral measurements were collected with an ASD FR spectrometer, averaged, and corrected to absolute reflectance using a NIST traceable

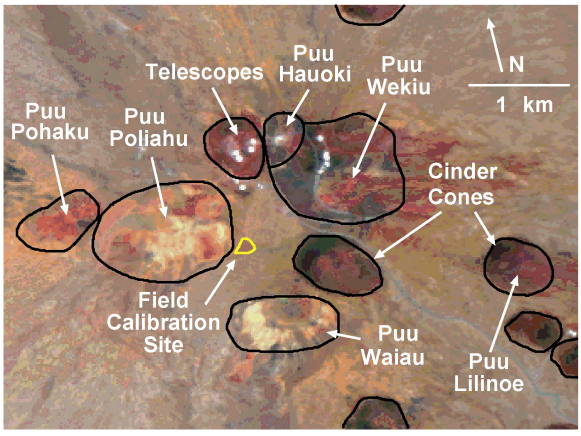

Figure 3. True color composite AVIRIS image of the summit of Mauna Kea. Cinder cones are circled in black and the field calibration site is circled in yellow. Strongly altered areas show up as bleached areas.

Figure 4. Collection of field calibration spectra at the base of the Puu Poliahu cinder cone near the summit of Mauna Kea. Erosion has exposed a zone of argillic alteration produced by a relict hydrothermal system seen as a bleached area.

spectralon reflectance correction. Shadowed areas below the SE margin of the Mauna Loa summit caldera (about 4000 m elevation) were used to derive a path radiance correction.

AVIRIS data calibrated to apparent reflectance were spectrally mapped using the USGS Tetracorder System (Clark et al., 2003). Tetracorder uses a modified least-squares band-shape fitting technique to spectrally identify materials and create maps of their distribution. The primary algorithm works by scaling a library spectrum to an observed spectrum using a modified least-squares solution to derive a numerical value called "*fit*." The algorithm derives *fits* for all of the spectra in its library and selects the material with the highest *fit* as the best spectral match. Comparisons are done only in the wavelength regions of diagnostic absorptions. In most cases Tetracorder identifies the spectrally-dominant material in each spectral region (e.g. electronic and vibrational), but it is capable of identifying mixtures if representative spectra of those mixtures are added to its library. When Tetracorder identifies a material as spectrally dominant that material does not have to be pure, it can also be intimately or aerially mixed with other phases. Spectral dominance means the diagnostic absorptions of that material are the strongest features in a given spectral region and are not obscured beyond recognition by absorptions from other phases. Other parameters like *depth* and *fit*depth* are determined for each comparison, and if the highest *fit*, *depth*, or *fit*depth* falls below a threshold then *no match* is found and the observed spectrum is not identified. Mineral maps of the electronic (0.4 - 1.35 μm) and vibrational (1.35 - 2.5 μm) spectral regions were produced for the entire flight line.

DISCUSSION

Types of Alteration

Alteration of mafic volcanic rocks can occur in a number of ways: 1) pervasive supergene alteration caused by weathering and oxidation of minerals when they are exposed to atmospheric oxygen, 2) widespread deuteric alteration related to degassing of the host lava or alteration caused by interaction with meteoric water or the atmosphere during emplacement of hot lava, and 3) localized hydrothermal alteration caused by hot fluids that circulate along fractures or other conduits after extrusion of the lava. These processes create a continuum of alteration mineral associations superimposed on each other. Supergene alteration cause by weathering forms palagonitic soils nearly devoid of phyllosilicates but containing nanocrystalline ferric oxide and hematite (Morris et al., 2001). Dueteric alteration may also lead to the formation of palagonite and various Fe-minerals. Hydrothermal alteration can usually be recognized by the presence of characteristic mineral associations that vary depending on the chemistry and temperature of the fluids, and composition of the host rock (Guilbert and Park, 1986). The types of hydrothermal alteration present on Mauna Kea and Mauna Loa are characteristic of the argillic and advanced argillic associations formed when hot, sometimes acidic, fluids or vapors percolate up through cinder cones or along caldera walls leaching iron from host rocks leaving bleached zones rich in clays like kaolinite, montmorillonite, ferruginous smectite, saponite, and in a few places hydroxysulfates like alunite and jarosite (Table 1). Ugolini (1974) investigated the altered materials from the summit cinder cones and found evidence of montmorillonite and saponite formed during hydrothermal alteration due to influx of hypogene fluids causing Mg-enrichment of saponite relative to non-hydrothermally altered tephra.

Table 1. Generalized chemical formulas for some clays and hydroxysulfates discussed in this paper.

Montmorillonite	$(Na,Ca_{0.5})_{0.33}(Al,Fe^{3+},Mg)_2Si_4O_{10}(OH)_2 \bullet nH_2O$
Ferruginous smectite	$(Na,Ca_{0.5})_{0.33}(Al,Fe^{3+},Mg)_2(Si,Al)_4O_{10}(OH)_2 \bullet nH_2O$
Nontronite	$(Na,Ca_{0.5})_{0.33}(Fe^{3+})_2(Si,Al,Fe^{3+})_4O_{10}(OH)_2 \bullet nH_2O$
Saponite	$(Na,Ca_{0.5})_{0.33}(Fe^{2+},Fe^{3+},Mg)_3(Si,Al)_4O_{10}(OH)_2 \bullet nH_2O$
Kaolinite	$Al_2Si_2O_5(OH)_4$
Alunite	$(Na,K,H_3O)Al_3(SO_4)_2(OH)_6$
Jarosite	$(Na,K,H_3O)Fe_3(SO_4)_2(OH)_6$

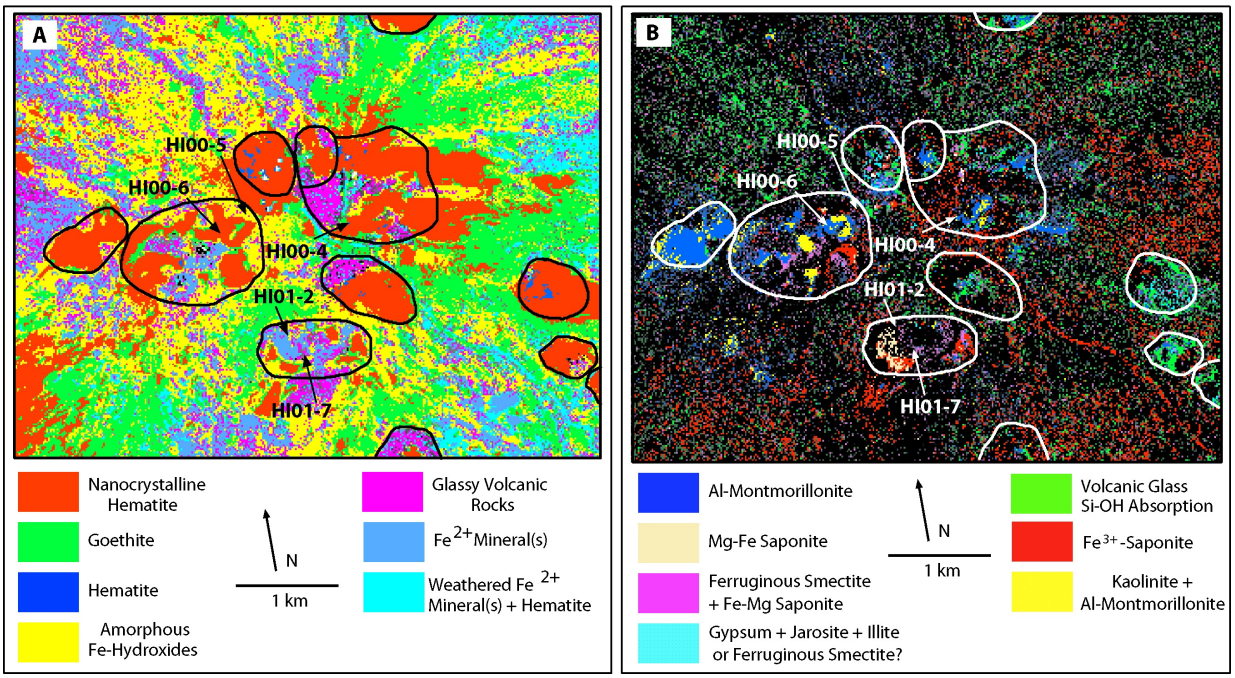

Figure 5. A) Electronic region (0.4 - 1.35 μm) minerals on the summit of Mauna Kea. Cinder cones are outlined in black. Arrows show collection locations of samples. B) Vibrational region (1.35 - 2.5 μm) minerals on the summit of Mauna Kea. Cinder cones are outlined in white.

Mauna Kea Mineral Maps

Five hydrothermally altered cinder cones were identified at the summit of Mauna Kea: Puu Pohaku, Puu Poliahu, Puu Hauoki, Puu Wekiu, and Puu Waiau. Formation of the Puu Waiau (107 ka) and Puu Poliahu (53 ka) cinder cones during the Pleistocene was subaerial and not subglacial as once believed with their once cone-like profiles rounded by subsequent glacial erosion (Wolfe et al., 1997). Alteration occurred during or soon after the eruptions that formed the cones. The mineral map of the electronic region shows that the cinder cone hydrothermal alteration is characterized by nanocrystalline hematite, hematite, goethite, and amorphous Fe-minerals in this spectral region (Fig. 5A). The hydrothermally altered cinder cones have the same types of Fe-minerals as non-hydrothermally altered cones and surrounding lava flows, therefore in this case Fe-mineralogy determined by AVIRIS cannot be used to distinguish between alteration as a result of supergene oxidation due to weathering and oxidation due to interaction with hydrothermal fluids.

The mineral map of the vibrational region shows the distribution of the alteration minerals more clearly. The hydrothermal alteration is characterized by zones of spectrally dominant kaolinite, Al-montmorillonite, ferruginous smectite, and saponite (Fig. 5B). The task of interpreting the relative positions of these mineral zones is made difficult because the alteration zones have been variably exposed by erosional dissection of the original cinder cone topography. Figure 6 shows a very generalized model of the relative sequence of spectrally determined mineral zones. Kaolinite + Al-montmorillonite alteration is limited in extent while the other alteration minerals are more widespread within the areas of hydrothermal alteration. The Al-montmorillonite zones (blue) usually enclose smaller kaolinite + Al-montmorillonite zones (yellow), and are themselves bordered, in places, by ferruginous smectite + Fe-Mg saponite zones

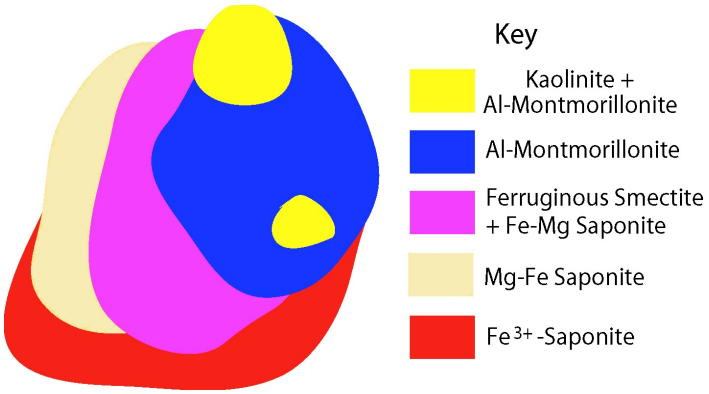

Figure 6. Idealized model of spectrally determined mineral zones.

(magenta) as seen on Puu Poliahu. On Puu Waiau a Mg-Fe saponite zone (tan) borders the southwestern side of a donut-shaped ferruginuous smectite + Fe-Mg saponite zone (Fig. 5B), which is bordered on the east by a Fe^{3+}-saponite zone (red). Nontronite-like Fe^{3+}-saponite is the only spectrally detectable clay widely dispersed among the non-hydrothermally altered volcanic rocks. The large bleached area on the western slope of Puu Waiau was initially identified as either saponite, hectorite, or talc because absorption features of these minerals look spectrally similar at AVIRIS spectral resolution. Analysis of field samples was needed to confirm that we were indeed mapping Mg-Fe saponite in this area (Fig 5B).

The absence of alunite is conspicuous at the spatial scale of AVIRIS on Mauna Kea and Mauna Loa when compared to alteration formed in continental settings, and may be explained by the possible lack of H_2S in Hawaiian magmatic gasses required for alunite formation near the surface (Robert Rye, personal comm.). Some alunite, however, has been identified in hand samples collected from the altered rocks of the Puu Poliahu cinder cone on Mauna Kea (Wolfe et al., 1997). Spectra from three pixels on this cinder cone did show possible evidence of alunite but its spectral features are nearly concealed by more abundant kaolinite. It is possible that the dry nature of tholeiitic magmas and rapid migration of meteoric water through highly porous volcanic rocks down to sea level and out into the ocean may not allow the formation of large circulating hydrothermal systems (Don Thomas, personal comm.). Indeed, it is the presence of clays produced by alteration of the Puu Waiau cone that has allowed surface waters to accumulate forming Lake Waiau in an otherwise arid landscape (Wolfe et al., 1997). Jarosite may also be present mixed with gypsum and illite on the slopes of Puu Lilinoe, but due to its marginal detection there in the AVIRIS data, this possible occurrence needs field verification.

Guinness et al. (2001) also spectrally analyzed the AVIRIS data acquired over Mauna Kea and found that the alteration systems in the cinder cones had central cores of montmorillonite, surrounded by saponite zones, in turn surrounded by outer kaolinite zones. Their findings differ from those discussed here by our identification of ferruginous smectite and only minor amounts of kaolinite. We were unable to detect kaolinite outside of the hydrothermally altered areas when we extracted spectra from pixels that corresponded to the areas they identified as containing kaolinite. Our field calibration site coincides with a cluster of kaolinite pixels on their map; examination of our field spectra revealed no spectrally detectable kaolinite. Apparently the kaolinite they mapped in unaltered rock was an artifact of simultaneously mapping ferric minerals in the 1-μm region and kaolinite in the 2-μm region using Spectral Angle Mapper that has been eliminated from their more recent maps (Guinness, pers com.). Two levels of verification were used to check the mineral maps: 1)

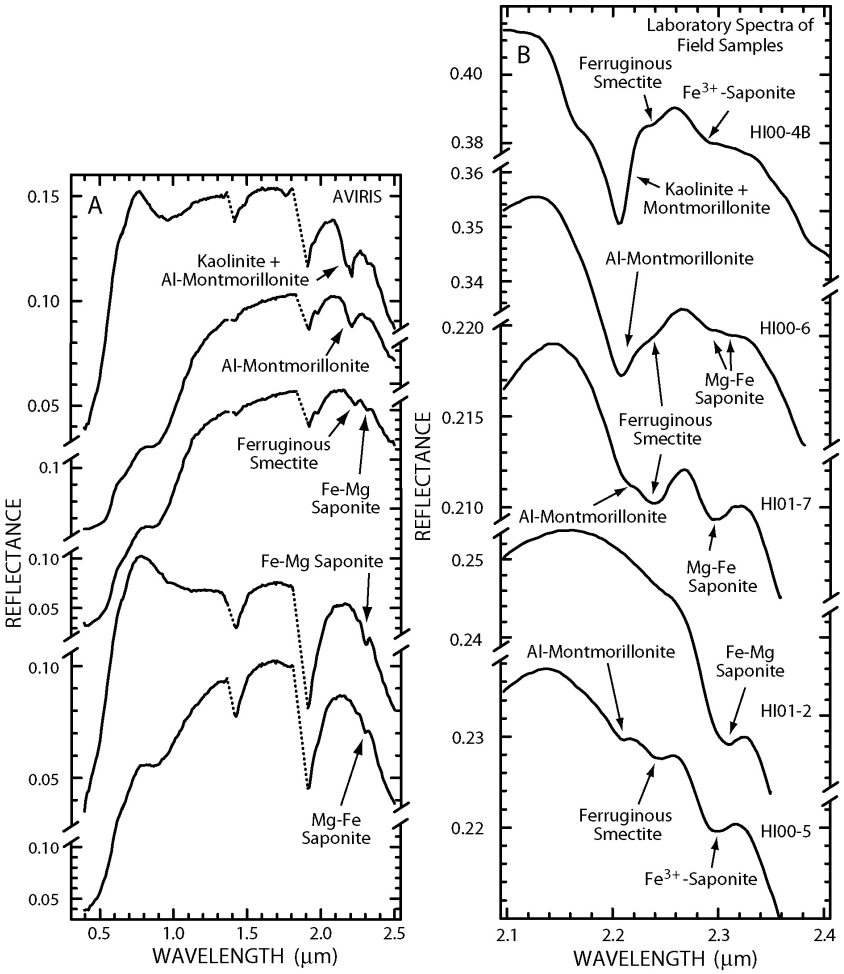

Figure 7. A) Averaged AVIRIS spectra extracted from alteration mineral zones in hydrothermal systems on Mauna Kea. Spectra offset vertically for clarity. B) Laboratory reflectance spectra of alteration minerals in field samples collected from the hydrothermal systems on Mauna Kea.

extraction and comparison of AVIRIS spectra to library spectra of well-characterized minerals, and 2) mineralogic analyses of field samples. Because of the remoteness of most areas in the flight lines comparison of extracted spectra to library spectra was used as the primary means of mineralogic verification of the mineral maps. Field samples were collected from hydrothermal systems on Puu Poliahu, Puu Waiau, and Puu Wekiu cinder cones (Fig. 3). Five samples from the alteration zones on Mauna Kea were subjected to X-ray diffraction analysis (XRD). These samples were also measured spectroscopically in the laboratory with results compared to those from XRD (see Fig. 7 and Table 2).

Table 2. Field sample verification of mineralogy derived from imaging spectroscopy.

Sample ID	Sample location			Tetracorder result	Verification
HI00-4F	N19 W155	49' 15" 28' 18"	West side Puu Wekiu Cinder Cone	**Nanocrystalline hematite**[1], **kolinite + Al-montmorillonite**	*XRD:* albite (M), microcline (m), smectite (m) consistent with **montmorillonite**, nontronite or saponite (m), **kaolinite** (tr). *LS*: **nanocyrstalline hematite** or goethite, **kaolinite, Al-montmorillonite**, Fe-saponite, ferruginous smectite.
HI00-6F	N19 W155	49' 17" 28' 55"	Northeastern Puu Poliahu	**Nanocrystalline hematite, Al-montmorillonite**	*XRD*:albite (M), microcline (m), smectite (m) consistent with **montmorillonite**, nontronite or saponite (tr), hematite (tr). *LS*: **nanocrystalline hematite, Al-montmorillonite**, ferruginous smectite, Mg-Fe saponite.
HI01-7	N19 W155	48' 37" 28' 46"	Western top of Puu Waiau	Glassy volcanics, **ferruginous smectite + Mg-Fe-saponite**	*XRD:* Anorthite (M), nontronite or **saponite** (m), **montmorillonite** (m), kaolinite (tr). *LS:* **ferruginous smectite, Mg-Fe saponite,** Al-montmorillonite.
HI01-2	N19 W155	48' 43" 28' 47"	Western slope of Puu Waiau	**Fe-minerals**, **Fe-Mg saponite**	*XRD:***saponite** from glycolation of clay separate. Main fraction not measured. *LS:* trace **Fe-minerals**, **Fe-Mg saponite**.
HI00-5F	N19 W155	49' 23" 28' 48"	Northeastern Puu Poliahu	Amorphous Fe-hydroxide, **Fe-saponite**	*XRD:*albite (M), microcline (m), **saponite** by glycolation of clay sep. (m), hematite(tr). *LS:* trace Fe-mineral(s)**, Fe-saponite,** ferruginous smectite, Al -montmorillonite.

XRD = X-ray diffraction analysis; *LS* = laboratory spectroscopy; clay sep. = clay separate; **bold** mineral names in "Tetracorder results" column also verified in field samples; (M) = major component 20wt% or more; (m) = minor 5-20 wt%; (tr) = trace < 5 wt%. [1]Trace hematite, goethite, jarosite and other Fe^{3+}-bearing minerals can be difficult for XRD to detect, even when red and yellow Fe^{3+} colors are present in the sample. Sample position is ± 50m (positions based on NAD83 datum).

Burns (1993, and references therein) suggest that deep weathering of mafic and vitric tuffs initially forms Fe^{2+}-saponite that subsequently oxidizes to partially dehydroxylated Fe^{3+}-Mg saponite, Fe^{3+}- montmorillonite, and nontronite intimately intergrown with ferrihydrite, nanocrystalline hematite, or FeOOH phases. A 2.232-μm band of variable strength often forms a shoulder or a completely independent absorption on the longward side of the 2.213-μm montmorillonite Al-OH combination band in many of the Mauna Kea samples, and may be caused by the presence of ferruginous smectite. In Fe-rich dioctahedral smectites some or all of the octahedral Al is replaced by Fe^{3+} with total replacement occurring in nontronites. The term ferruginous smectite applies to dioctahedral smectites when $Fe^{3+} > 3\%$ whereas montmorillonites have $Fe^{3+} < 1\%$ (Frost and Kloprogge, 2000). Ferruginous smectite may be an Fe-montmorillonite equivalent formed by oxidation and dehyroxylation of the Fe^{2+}-saponite on Mauna Kea. Both saponite and ferruginous smectite (a.k.a. Fe-montmorillonite) are present in variable proportions in nearly all of the samples collected from the Mauna Kea alteration systems (Fig. 7B) at concentrations much higher than in the surrounding non-hydrothermally altered rock (Fig. 5B). Burns suggest that intracrystalline oxidation of

Fe^{2+} to Fe^{3+} in cation clusters with metal vacancies creates additional absorptions that can form shoulders on the main combination bands in the 2 - 2.5 μm region resulting in broader but weakened absorptions that might be difficult to identify with remote sensing. Dehydration may also be an important mechanism for reducing H_2O-related band strengths in ferrihydrite-bearing smectites (Bishop et al., 1993). A combination of both mechanisms may be at work in the saponites and ferruginous smectites observed at Mauna Kea as their absorption bands rarely have depths greater than a few percent but XRD indicates abundances of 5 - 20 wt% in these relatively bright soils with 20 - 40% reflectance in the 2- 2.5 μm region. Nanocrystalline hematite and ferrihydrite have been identified in individual samples of palagonitized tephra and soil from Mauna Kea (Morris et al., 1993, 2001; Golden et al., 1993). The apparent lack of ferrihydrite at the spatial scale of AVIRIS may be explained by its tendency to dissolve and reprecipitate as goethite (Bigham et al., 1992), its spectral obscurity when intimately mixed with other Fe-minerals, or its nanocrystalline character (Morris et al., 1996) causing it to be classified into the more generic amorphous Fe-hydroxides category.

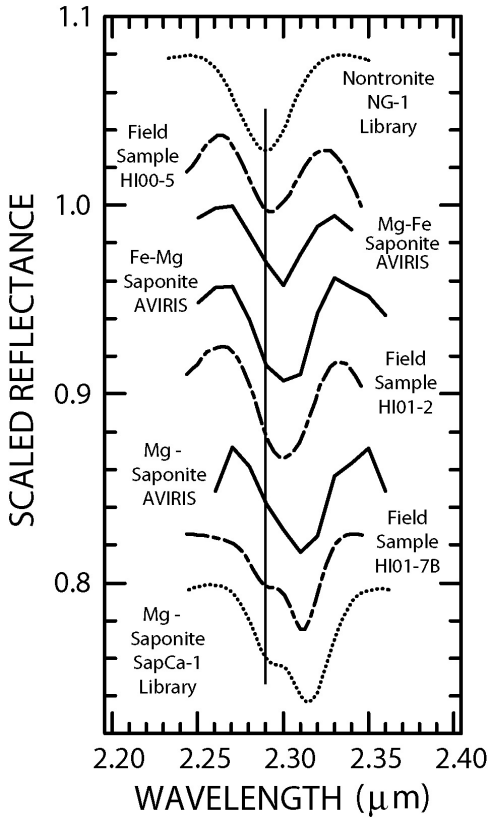

Figure 8. Comparison of continuum-removed absorptions from spectra of nontronite and saponites. Vertical line is a reference from which to measure the wavelength shift of the band centers. Spectra offset vertically for clarity.

Spectrally differentiating between nontronite and Fe^{3+}-saponite is difficult because their diagnostic absorptions overlap in some cases. Mg-rich saponites have an Fe-OH combination band that forms a shoulder at 2.292 μm (see sample SapCa-1in Fig.8) on the short wavelength side of the 2.312 μm Mg-OH combination band. This shoulder and absorptions at intermediate wavelength positions may be due to octahedral layer hydroxyl groups adjacent to cation clusters with vacancies (V) like $Fe^{3+}Fe^{3+}$(V), $MgFe^{3+}$(V), and fully occupied clusters like $MgFe^{2+}Fe^{3+}$ formed by the intracrystalline oxidation described above. Oxidized Fe-Mg saponite has two bands at intermediate positions between these endmember band positions that overlap significantly forming one broad composite absorption centered at 2.305 μm (e.g. see sample HI01-2 in Fig. 8). The spectrum of sample HI00-5 has a 2.292-μm absorption at the same wavelength position as that of nontronite (source clay mineral standard NG-1) but is missing an Mg-OH absorption at 2.312 μm. Differentiation was equally challenging using XRD on non-glycolated samples because of over-lapping saponite and nontrontite peaks. Thinking this sample contained nontronite we tested for the presence of saponite by analyzing a glycolated clay separate of this sample with XRD. Saponite was identified as the dominant smectite in the glycolated clay fraction of both HI00-5 and HI01-2 based on the appear-ance of a peak at 10.5° 2θ characteristic of glycolated saponite and lacking in the other smectites. Spectroscopy suggests the presence of nontronite in HI00-5 while XRD indicates saponite; perhaps this is evidence of an intermediate di- and tri-octahedral nontronite-like Fe^{3+}-saponite phase in this sample (Guven, 1988). Thus it appears that Fe^{3+}-saponite produced by intracrystalline oxidation is geochemically and spectrally a defacto nontronite with the original crystal lattice of a trioctahedral Fe^{2+}-saponite. It is possible to detect compositional variations of saponite with AVIRIS (see Fig. 5B). The spectral map key is coded to indicate the spectrally dominant cation in saponite: Fe^{3+}-, Mg-Fe, Fe-Mg, and Mg-saponite categories are listed here in order of increasing Mg content. It may be that Fe^{2+}-saponite is oxidized to Fe^{3+}-saponite where there is no hydrothermal Mg-enrichment, possibly accounting for the observed widespread nontronite-like 2.29-μm spectral signatures outside of the hydrothermally altered areas (Fig. 5B) in weathered rocks. In contrast, Mg-rich saponite, like kaolinite, may be indicative of hydrothermal alteration on Mars.

A tentative model for the alteration zones present in the summit cinder cones on Mauna Kea is presented in Fig. 9. This model was constructed from the mineral assemblages present in the vibrational mineral map (Fig. 5B) and spectra of field samples (Fig. 7B). Multiple clay phases exist in variable proportions in nearly all of the samples, therefore the alteration mineral associations were arranged into zones named after the spectrally dominant mineral

phase. The recognition of an alunite zone is based on the reported presence of alunite in the kaolinite zones on Puu Poliahu and assumes these occurrences are not of supergene origin. Similarly, if the ferruginous smectite was formed after hydrothermal alteration by oxidation of Fe^{2+}-saponite then this mineral may form a thin veneer over saponite-rich altered tephra. Clearly, additional field work is needed to substantiate the hydrothermal origin of the ferruginous smectite. The complex overlap of alteration zones may indicate multiple centers of short-lived hydrothermal activity that migrated frequently. However, the mineral assemblages recognized in spectra of the field samples (Fig. 7B) suggest a consistent geochemical trend, where hot acidic hydrothermal fluids spread outward, forming alunite and kaolinite until they became cooler and less acidic through reaction with the surrounding host rock. As these less-acidic hydrothermal fluids continued outward they formed Al-montmorillonite, and then Fe-rich ferruginous smectite, and eventually Fe-Mg saponite which itself became progressively more Mg-rich toward the edges the altered areas. High temperature, among other factors, favors substitution of Al over Fe in muscovite (Duke, 1994). A similar trend may be apparent where Al-rich montmorillonite becomes progressively more Fe-rich, eventually becoming ferruginous smectite away from the most intensely altered areas.

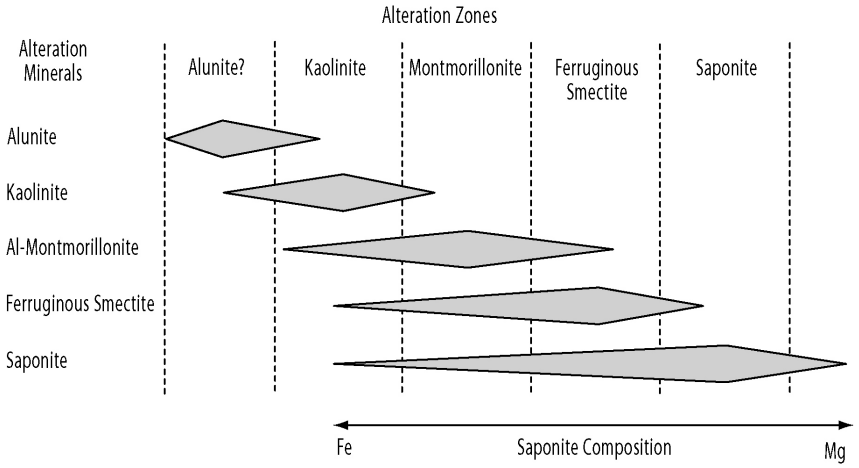

Figure 9. A model proposed for hydrothermal alteration zones on Mauna Kea.

Mauna Loa Mineral Maps

One small area of hydrothermally altered rock was recognized on the western caldera wall of Mauna Loa just below the summit (Figs. 2, 10, and 11) covering an area of about 0.006 km^2. This area is spectrally dominated by nanocrystalline hematite, goethite, kaolinite, Al-montmorillonite, and jarosite, a mineral association that is typical of advanced argillic alteration, which implies formation in a hydrothermal system. Field observations confirm that similar active, small, caldera-wall hydrothermal systems exist on the even younger Kilauea volcano (directly east of Mauna Loa). The shield-building stage hydrothermal systems responsible for these small altered zones are dwarfed by the relatively larger systems (0.06 - 0.3 km^2) associated with the more volatile-rich postshield stage cinder cones on Mauna Kea. The mineral map of the electronic region (Fig. 10A) shows that the recent basalt flows (labeled "**5**") become progressively more weathered in a down slope direction probably due to higher moisture at lower elevations where hematite gives way to goethite. Nanocrystalline hematite apparently forms during weathering in more humid areas at lower elevations on the flanks and also on the NW side of the summit of Mauna Loa where afternoon clouds build. The Fe^{3+}-minerals formed from weathering of the tholeiitic basalts on Mauna Loa are for the most part nanocrystalline based on their relatively weak 0.65-0.7 μm bands, and it is possible that what was mapped as nanocrystalline hematite may be a mixture of nanocrystalline Fe-bearing phases including hematite, ferrihydrite, and goethite.

It is possible to establish an eruptive chronology based on spectrally-detected mineralogy. Comparison of the mineral maps (Figs. 10 and 11) with the geologic map of Mauna Loa (Wolfe and Morris, 1996) allowed placement of numbers corresponding to the relative ages of the basalt flows on the mineral maps. This exercise helped clarify several interesting mineralogic patterns. In the electronic spectral region, the youngest flows retain their mafic surface mineralogy of spectrally detectable olivine and pyroxene (Fig. 12), whereas the surfaces of older flows are dominated by Fe-oxide and hydroxide minerals formed by weathering (Fig 10A). The weathering sequence is elevation-dependent with the youngest flows at the summit characterized by pyroxene+olivine and glassy volcanic rock, the intermediate-aged flows characterized by hematite and weathered Fe^{2+}-minerals + hematite, and the oldest flows characterized by nanocrystalline hematite. At lower elevations older flows are also characterized by amorphous Fe-hydroxides. Relatively recent (< 0.2 ka) flows on the N flank of Mauna Loa, just above the 2000 m contour near Humuula saddle, and on the SW flank, have a blue iridescence caused by a peak in reflectance at 0.41

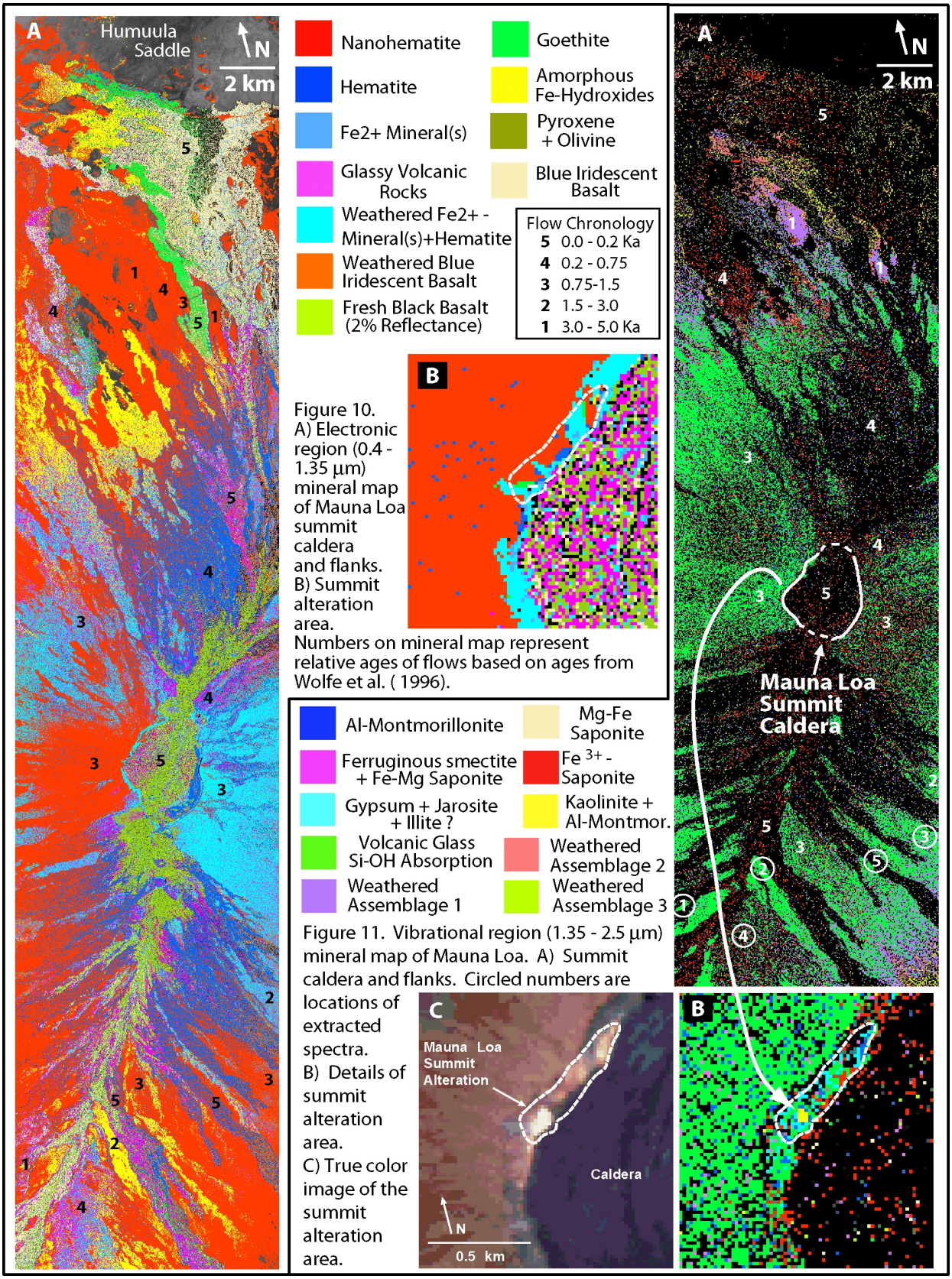

Figure 10. A) Electronic region (0.4 - 1.35 µm) mineral map of Mauna Loa summit caldera and flanks. B) Summit alteration area. Numbers on mineral map represent relative ages of flows based on ages from Wolfe et al. (1996).

Figure 11. Vibrational region (1.35 - 2.5 µm) mineral map of Mauna Loa. A) Summit caldera and flanks. Circled numbers are locations of extracted spectra. B) Details of summit alteration area. C) True color image of the summit alteration area.

μm (Fig. 13) reminiscent of the diffraction scattering peak seen at ultraviolet wavelengths in common opal and at visible wavelengths in precious opal (Darragh et al., 1976). The blue iridescence appears to be related to the initial stages of basalt weathering in the relatively moist environment at lower elevations because spectra of the same flows at higher elevations (> 3000 m) on the mountain and older flows (> 0.7 ka) at lower elevations have no peaks.

In the vibrational spectral region, older flows show spectral evidence of a 2.24-μm Si-OH absorption probably related to hydration of basaltic glass whereas the younger flows lack this spectral feature (Fig.14). A possible explanation is that over time, water diffuses into the surface of a flow forming a water-rich hydration rind that increases in thickness with time. Studies have shown that growth of hydration rinds is a non-linear function of time, relative humidity, temperature, and lava composition (Friedman and Smith, 1960, Friedman and Obradovich, 1981, Friedman et al., 1994). Various techniques have been developed to date obsidian archeological artifacts using the thickness of hydration rinds as an indicator of relative age. Based on analysis of the mineral patterns in Fig. 11A, it appears that spectral maps of the Si-OH absorption can be used to perform the same type of relative dating using hyperspectral data collected by airborne or orbital instruments. Hydration rinds are either spectrally concealed or destroyed by accelerated weathering at lower, more humid, elevations below about 2600 m on the N and SW flanks of Mauna Loa. A comparable mineral map pattern of Si-OH absorptions is absent at the summit of Mauna Kea probably because of the relatively older (generally >10,000 years based on the geologic map of Wolfe and Morris, 1996) and more weathered flows exposed there (Fig 5B). Possible application of this technique to date Martian lava flows would depend on how fast volcanic glass hydrates in the cold-thin atmosphere of Mars. The spectral signature of hydrated volcanic glass is similar to those of chert, chalcedony, opal, hydrated cristobalite, and coesite in the 2.2 - 2.3 μm region, but can be differentiated with adequate spectral resolution and signal-to-noise ratio. This is a potentially important distinction to make when searching for hydrothermally-altered areas on Mars.

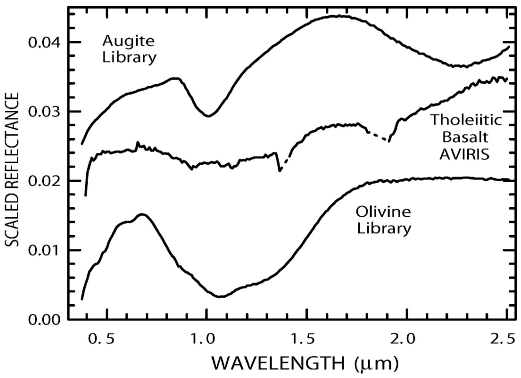

Figure 12. Averaged AVIRIS spectra extracted from an area where a recent flow (< 0.1 Ka) near the summit of Mauna Loa (Fig. 10A) that mapped as pyroxene + olivine compared to library spectra of pyroxene (augite) and olivine. The intimate mixture of these two minerals can explain the broad upward sloping absorption seen in the AVIRIS spectrum.

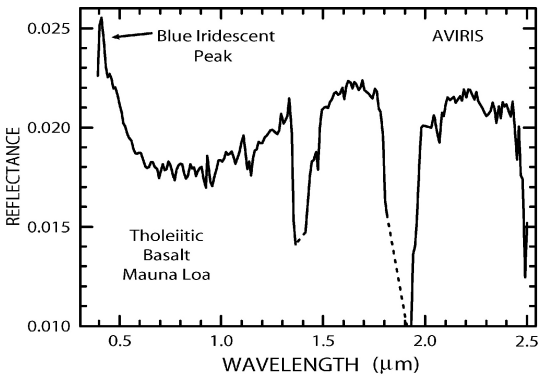

Figure 13. Averaged AVIRIS spectra extracted from a portion of a recent flow (< 0.2 Ka) on the NW flank of Mauna Loa just above the saddle that mapped as weathered blue iridescent basalt (Fig.10A).

Hydrothermal Alteration as a Function of Tectonic Setting

Over the past two decades geologists have analyzed hyperspectral data collected over 15 relict and 3 active hydrothermal systems ranging from those developed on hot spot shield volcanos, to those on continental margin stratovolcanos and continental interior calderas (Goetz and Strivastava, 1985; Kruse and Huntington, 1990; Simon, 1990; Swayze et al., 1992; King et al., 1995; Kruse et al., 1996; Crowley and Zimbelman, 1997; Swayze, 1997; Livo et al., 1999; Dalton et al., 2000; Rockwell et al., 2000; Martinez-Alonso, 2000; Smailbegovic et al., 2001; Martini et al., 2001; Vaughan et al., 2001). Some useful patterns emerge when the characteristics of hydrothermal systems developed in these three tectonic environments are compared (Fig. 15). It is apparent that the composition and volatile content of magmas influence the duration, mineral associations, size, and geometry of hydrothermal systems with drier, more mafic, magmas producing smaller, short-lived hydrothermal systems and wetter, more silicic, magmas producing larger, long-lived systems characteristic of continental interior calderas. Most notable is the

greater diversity of spectrally detectable alteration minerals, including alunite, and the presence of large propylitic zones and silica caps in hydrothermal systems of the continental interior calderas compared to the handful of alteration minerals, little to no alunite, and lack of propylitic zones or silica caps in hydrothermal systems on shield volcanos. In summary, very small hydrothermal systems develop along fault bounded caldera walls of tholeiitic basalt shield volcanos during the shield-building stage as seen at Mauna Loa and Kilauea. Small systems develop in summit and flank cinder cones during the postshield-building stage of alkalic volcanism on shield volcanos as seen at Mauna Kea. Medium-sized hydrothermal systems develop at the summits and on the flanks of andesitic stratovolcanos along subduction margins as seen at Mt. Rainer (Crowley and Zimbelman, 1997) and the Nansatsu District in Japan (Hedenquist et al., 1994). And large hydrothermal systems develop in or along the margins of continental interior bimodal rhyolite/basalt calderas as seen at Cuprite (Swayze, 1997) and Goldfield, Nevada (Ashley and Silberman, 1976).

There are exceptions to these trends with large continental interior-style hydrothermal systems occurring in subduction margin island arcs like the Philippines (Reyes, 1990). Likewise, many of the alteration minerals observed in hydrothermal systems of continental interior calderas are present in the subduction margin systems but at spatial scales too small to spectrally dominate entire pixels.

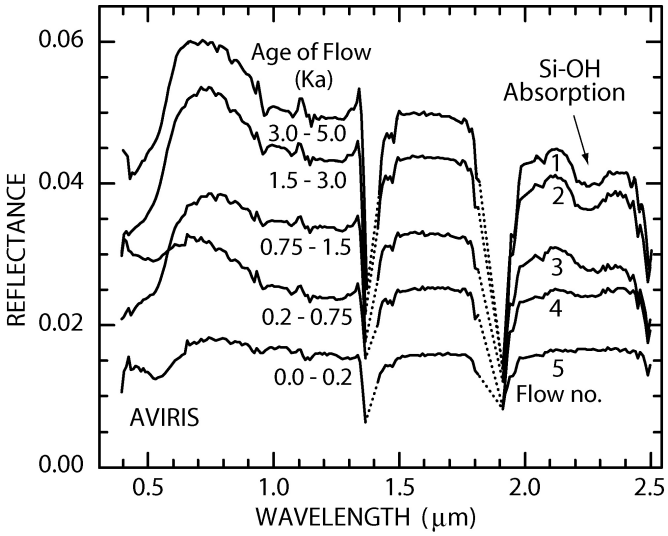

Figure 14. Averaged AVIRIS spectra of tholeiitic basalt flows of different age from the southwestern flank of Mauna Loa. Spectra were extracted from sites shown in Fig. 11A (circled numbers). Note that older flows have deeper 2.24-μm Si-OH absorptions. 1.0 Ka = one thousand years ago.

Tectonic Setting	Oceanic Hotspot Shield Volcanoes	Subduction Margin Stratovolcanoes	Continental Interior Calderas
Magmatic Composition	Mafic	Intermediate	Silicic
Volcanic Rock Composition	Tholeiitic Basalt	Andesite	Bimodal Rhyolite / Basalt
Magmatic Volatile Content	Dry		Wet
Structural Setting	Caldera Basins & Walls Rift Zones & Cinder Cones	Volcanoe Summit and Flanks	Caldera Basins & Margins
Duration of Hydrothermal Centers	Few Years to Decades	1000 - 10,000 Years	Up to Millions of Years
Spectrally Detectable Alteration Mineral Associations (0.4 - 2.5 microns) at > 14x14 m pixel scale	Cristobalite Goethite Gypsum Hematite Jarosite Kaolinite + smectite Al-Montmorillonite Ferruginous Smectite Saponite	Alunite Chlorite Cristobalite Cryptocrystalline Quartz Goethite Gypsum Hematite Jarosite Kaolinite Montmorillonite Opal Sericite/Illite Smectite	Alunite Buddingtonite Chlorite Chalcedony Cristobalite Dickite Goethite Gypsum Halloysite Hematite Jarosite Kaolinite Montmorillonite Opal Pyrophyllite Sericite/Illite Smectite
Size of Hydrothermal Centers	0.006 - 0.3 km ^{2}	1 - 8 km^2	2-10 km^2
Geometry of Hydrothermal Centers	No Silica Cap No Alunite Zones No Propylitic Zones	Some Silica Caps Small Alunite Zones Propylitic Zones	Large Silica Cap Large Alunite Zones Propylitic Zones
Spectral evidence of acid-sulfate alteration (at > 14 x 14 m pixel scale)	Absent		Abundant

Figure 15. Hydrothermal alteration as a function of host rock composition, tectonic setting, and magmatic volatile content.

THE SEARCH FOR MARTIAN HYDROTHERMAL SYSTEMS

The spectral search for alteration minerals will undoubtably continue to play a critical role in the search for relict hydrothermal systems on Mars (Farmer, 1996). Results of this study suggest that the classical set of alteration mineral associations found in active continental interior calderas like Yellowstone, Wyoming or relict systems like Goldfield, Nevada, are not all likely to be found in Martian volcanic hydrothermal systems given the lack of comparable tectonic settings on Mars. Alternatively, the Hawaiian alteration mineral

associations are probably closer to what we should expect to find on Mars. Alteration minerals such as chalcedony, chlorite, dickite, halloysite, opal, pyrophyllite, and sericite are absent in the Hawaiian systems at the spatial scale of AVIRIS (14 m pixels). The presence of only small hydrothermal systems on Hawaii at the surface may be an observation biased by what is exposed. Larger systems formed at depth, if they exit, have little chance of being exposed due to rapid subsidence of the islands (Don Thomas, personal comm.). If large hydrothermal systems have developed at depth on Mars, they may have been subsequently exposed by erosion, edifice collapse, or exhumation during meteorite impact.

Successfully locating Martian hydrothermal systems will require the identification of alteration minerals with enough spectral contrast to avoid confusion with minerals formed by weathering in non-hydrothermally altered areas. Unfortunately many of the alteration minerals found in the Hawaiian hydrothermal systems also form during weathering of mafic volcanic rocks. Nontronite-like Fe^{3+}-saponite is a weathering product of the non-hydrothermally altered basaltic rocks surrounding the hydrothermal centers on Mauna Kea (Fig. 5B). Similarly hematite and goethite form as products of weathering of non-hydrothermally altered sulfide-rich volcanic rocks on both mountains (Figs 5A and 10A). The most reliable indicator of hydrothermal alteration in mafic volcanic rocks, from a remote sensing perspective, is the presence of kaolinite. It is present in the hydrothermal centers on both Mauna Kea and Mauna Loa, in the most intensely altered areas. The process of hydrothermal alteration must hasten the formation of Fe^{2+}-saponite from basaltic rocks with resulting oxidation and dehyroxylation to form Fe^{3+}- and Mg-saponites, and ferruginous smectite. Although this assemblage is normally present in weathered basalts (Burns, 1993), it seems that hydrothermal action may enhance the weathering process, creating areas with higher than background concentrations of these minerals. And if the mineral associations in the cinder cones on Mauna Kea are an applicable spectral analogue, then Mg-rich saponites may also be indicative of hydrothermal alteration on Mars. Care must be exercised to avoid potential confusion between the spectral signatures of hydrated volcanic glass, which might be widespread on Mars, and hydrated SiO_2 minerals indicative of localized hydrothermal alteration systems.

The duration of activity in a hydrothermal system also varies as a function of tectonic setting, lasting a few orders of magnitude longer in more silicic magmatic systems like those formed in continental interior calderas (Fig. 15). It seems logical that long-lived hydrothermal systems would provide a better shelter for Martian life and may be more likely to preserve evidence of that life than short-lived systems. This observation has important implications for the search for past life on Mars: the largest and best-developed hydrothermal systems may be those associated with postshield basalts or andesites on Mars. Cinder cones and exhumed altered rocks formed during the postshield stage of volcanism may be the best targets for remote detection of hydrothermal systems and for exobiology sample collection missions. These would be the areas to concentrate on in the search for sample return sites at spatial resolutions no coarser than 30 meters. Exopalaeontological studies may also benefit from studying the biota of active and relict hot springs of the Hawaiian and Icelandic oceanic hotspot hydrothermal systems. Areas of reduced permeability may be necessary for the formation of large hydrothermal convection cells at the surface.

Volcanism may not be the only mechanism for forming hydrothermal systems on Mars. Newsom (1980) has suggested that hydrothermal systems may have developed in meteorite impact melt sheets on Mars. Studies of terrestrial impact structures in continental settings have found evidence of extensive long-lived hydrothermal systems and their associated calc-silicate alteration mineral associations (McCarville and Crossey, 1996). For the same reasons discussed above, host-rock composition may influence the type of alteration minerals formed during impact induced heating. Unfortunately, terrestrial analogues of impact-driven hydrothermal alteration applicable to Martian mafic volcanic rocks may not exist because plate subduction has probably destroyed the oceanic impact structures they reside in, biasing the terrestrial geologic record toward those preserved in silicic cratons. Nevertheless, the alteration minerals formed in the hydrothermal systems on Mauna Kea and Mauna Loa may be useful guides in deducing the effects of heat and water on mafic rocks expected during impact heating.

ACKNOWLEDGMENTS

Special thanks is given to Robert O. Green and the AVIRIS team for collecting and providing the imaging data. Ideas were clarified by helpful discussions with Trude King, Jim Crowley, Bob Tilling, Don Thomas, Sara Martinez-Alonso, Ed Guinness, Dick Morris, Ray Arvidson, Geoff Plumlee, Charlie Alpers, Skip Cunningham, and Blair Jones. The manuscript benefitted greatly from reviews by Eric Livo, Robert Rye, and Todd Hoefen. Funding was provided by the USGS Minerals Program. Any use of trade, product, or firm names in this publication is for descriptive purposes only and does not imply endorsement by the U.S. Government.

REFERENCES

Allen, C.C., J.L. Gooding, M. Jercinovic, and K. Keil, Altered basaltic glass: A terrestrial analog to the soil of Mars, *Icarus, 45*, 347-369, 1981.

Allen, C.C., J.L. Gooding, K. Kiel, Hydrothermally altered impact melt rock and breccia: Contributions to the soil of Mars, *Journal of Geophysical Research, 87*, 10083-10101, 1982.

Ashley, R.P., and M.L. Silberman, Direct dating of mineralization at Goldfield, Nevada, by Potassium-Argon and fission-track methods, *Economic Geology*, *71*, 904-924, 1976.

Bigham, J.M., U. Schwertmann, L. Carlson, Mineralogy of precipitates formed by the biogeochemical oxidation of Fe(II) in Mine Drainage, *in* Biomineralization: Processes of Iron and Manganese, H.C.W. Skinner, R.W. Fitzpatrick (eds.), *Catena Supplement 21*: Cremlingen-Destedt, Germany, 219-232, 1992.

Bishop, J.L., C.M. Pieters, R.G. Burns, Reflectance and Mössbauer spectroscopy of ferrihydrite-montmorillonite assemblages as Mars soil analog materials, *Geochimica et Cosmochimica Acta, 57*, 4583-4595, 1993.

Burns, R.G., Rates and mechanisms of chemical weathering of ferromagnesian silicate minerals on Mars, *Geochimica et Cosmochimica Acta, 57*, 4555-4574, 1993.

Clark, R.N., G.A. Swayze, K. E. Livo, R.F. Kokaly, S.J. Sutley, J. B. Dalton, R.R. McDougal, and C. A. Gent, Imaging spectroscopy: Earth and planetary remote sensing with the USGS Tetracorder and Expert Systems, *J. Geophys. Res.*, 2003, in press.

Clark, R.N., G.A. Swayze, K.E. Livo, R.F. Kokaly, T.V.V. King, J.B. Dalton, J.S. Vance, B.W. Rockwell, T. Hoefen, R.R. McDougal, Surface reflectance calibration of terrestrial imaging spectroscopy data: a tutorial using AVIRIS, Proceedings of the Eleventh JPL Airborne Earth Science Workshop, *Jet Propulsion Laboratory Publication*, this volume, 2003.

Clague, D.A., G.B. Dalrymple, The Hawaiian-Emperor volcanic chain. Part I. Geologic evolution, chap. 1 of R.W. Decker, T.L. Wright, P.H. Stauffer (eds.), Volcanism in Hawaii*: U.S. Geological Survey Professional Paper 1350, 1*, 5-54, 1987.

Clague, D.A., G.B. Dalrymple, Tectonics, geochronology, and origin of the Hawaiian-Emperor Chain *in* E.L. Winterer, D.M. Huson, R.W. Decker (eds.), The eastern Pacific Ocean and Hawaii, v. N *of* The geology of North America, Geological Society of America, 188-254, 1989.

Crowley, J.K., D.R. Zimbelman, Mapping hydrothermally altered rocks on Mount Rainier, Washington, with Airborne Visible/Infrared Imaging Spectrometer (AVIRIS) data, *Geology, 25*(6), 559-562, 1997.

Dalton, J.B., T.V.V. King, D.J. Bove, R.F. Kokaly, R.N. Clark, J.S. Vance and G.A. Swayze, Distribution of acid-generating and acid-buffering minerals in the Animas River Watershed as determined by AVIRIS spectroscopy, *Proceedings of the ICARD 2000 Meeting*, Denver Colorado, 1541-1550, 2000.

Darragh, P.J., A.J. Gaskin, J.V. Sanders, Opals, *Scientific American, 234(4)*, 84-95, 1976.

Duke, E.F., Near infrared spectra of muscovite, Tschermak substitution, and metamorphic reaction progress: implications for remote sensing, *Geology*, *22*, 621-624, 1994.

Evans, D.L., J.B. Adams, Composition of Viking Lander multispectral images and laboratory reflectance spectra of terrestrial samples, *Proc. Lunar Planet. Sci. Conf., 10th*, 1829-1834, 1979.

Evans, D.L., J.B. Adams, Amorphous gels as possible analogs to martian weathering products, *Proc. Lunar Planet. Sci. Conf. 11th*, 757-763, 1980.

Farmer, J.D., D.J. De Marais, Exopaleontology and the search for a fossil record on Mars, *Lunar Planet. Sci., 25*, 367-368, 1994.

Farmer, J.D., Hydrothermal systems on Mars: an assessment of present evidence, in Evolution of hydrothermal ecosystems on Earth (and Mars?), *Ciba Foundation Symposium 202*, Wiley and Sons, 273-299, 1996.

Friedman, I., R.L. Smith, A new dating method using obsidian: Part I, The development of the method., *American Antiquity, 25*, 476-522, 1960.

Friedman, I., J. Obradovich, Obsidian hydration dating of volcanic events, *Quaternary Research, 16*, 37-47, 1981.

Friedman, I., F.W. Trembour, F.L. Smith, and G.I. Smith, Is obsidian hydration dating affected by relative humidity? Quaternary Research, 41(2), 185-190, 1994.

Frost, R.L., J.T. Kloprogge, Vibrational spectroscopy of ferruginous smectite and nontronite, *Spectrochimica Acta Part A, 56*, 2177-2189, 2000.

Gao, B-C, K.B. Heidebrecht, and A.F.H. Goetz, Derivation of scaled surface reflectances from AVIRIS data, *Remote Sensing of Environment, 44(2)*, 165-178, 1993.

Goetz, A.F.H., and Vinay Strivastava, Mineralogical mapping in the Cuprite mining district, Proceedings of the Airborne Imaging Spectrometer (AIS) Data Analysis Workshop, *Jet Propulsion Laboratory Publication 85-*

41, 22-29, 1985.

Golden, D.C., R.V. Morris, and D.W. Ming, Mineralogy of three slightly palagonitized basaltic tephra samples from the summit of Mauna Kea, Hawaii, *J. Geophys. Res., 98(E2)*, 3401-3411, 1993.

Guinness, E.A., R.E. Arvidson, B.L. Ljolliff, R.V. Morris, and D.W. Ming, Mapping alteration minerals exposed on the summit of Mauna Kea Volcano using AVIRIS data: implications for mapping Mars mineralogy, Lunar and Planetary Science XXXII, 1659.pdf, 2001.

Guven, N., Smectites, in Hydrous Phyllosilicates, Reviews in Mineralogy, v. 19, chapter 13, S.W. Bailey (ed.), Mineralogical Society of America, 497-559, 1988.

Guilbert, J.M., C.F. Park, Jr., Ore Deposits, W.H. Freeman and Company, New York, 985pp., 1986.

Hedenquist, J.W., E. Izawa, N.C. White, W.F. Giggenbach, M. Aoki, Geology, geochemistry, and origin of high sulfidation Cu-Au mineralization in the Nansatsu District, Japan, *Economic Geology, 89(1)*, 1-30, 1994.

King, T.V.V., R.N. Clark, C. Ager, G.A. Swayze, Remote mineral mapping using AVIRIS data at Summitville, Colorado, and the adjacent San Juan Mountains: in Proceedings: Summitville Forum '95, eds. H.H. Posey; J.A. Pendelton; and D. Van Zyl, *Colorado Geological Survey Special Publication 38*, 59-63, 1995.

Kruse, F.A., K.S. Keirein-Young, and J.W. Boardman, Mineral mapping at Cuprite, Nevada with a 68-channel imaging spectrometer, *Photogrammetric Engineering and Remote Sensing*, *56*(1), 83-92, 1990.

Kruse, F.A., J.H. Huntington, The 1995 AVIRIS geology group shoot, Proceedings form the Airborne Earth Science Workshop, Jet Propulsion Publication, 1996.

Livo, K.E., R.N. Clark, F.A. Kruse, and R.F. Kokaly, Characterization of hydrothermally altered rock and hot spring deposits at Yellowstone National Park using AVIRIS data, Summaries of the Eight JPL Airborne Science Workshop, *Jet Propulsion Laboratory Publication 99-17*, 259-266, 1999.

Martinez-Alonso, S.E., Study of the infrared spectra of phyllosilicates through direct measurements, quantum mechanical modeling, and analysis of AVIRIS imaging spectrometer data: relationships with environment of mineralization, Ph. D. Dissertation, University of Colorado Boulder, 232 pp., 2000.

Martini, B.A., E.A. Silver, D.C. Potts, Hyperspectral remote sensing in Long Valley Caldera: issues of scale resolution, and signal to noise, Proceedings of the Tenth JPL Airborne Earth Science Workshop, *Jet Propulsion Laboratory Publication 02-1,* 275-282, 2001.

McCarville, P., L.J. Crossey, Post-impact hydrothermal alteration of the Manson impact structure, *Geological Society of America Special Paper 302*, 347-376, 1996.

Moore, J.G. D.A. Clague, W.R. Normark, Diverse basalt types from Loihi Seamount, Hawaii: *Geology, 10(2)*, 88-92, 1982.

Moore, J.G., D.A. Clague, Volcano growth and evolution of Island of Hawaii: *Geological Society of America Bulletin, 104(11)*, 1471-1484, 1992.

Morris, R.V., D.C. Golden, J.F. Bell, H.V. Lauer, and J.B. Adams, Pigmenting agents in Martian soils: Inferences from spectral, Mossbauer, and magnetic properties of nanophase and other iron oxides in Hawaiian palagonitic soil PN-9, *Geochimica et Cosmochimica Acta, 57*, 4597-4609, 1993.

Morris, R.V., D.W. Ming, D.C. Golden, J.F. Bell, III, An occurrence of jarositic tephra on Mauna Kea, Hawaii: Implications for the ferric mineralogy of the Martian surface, *in* Mineral Spectroscopy: A Tribute to Roger G. Burns, Geochemical Society special Publication No.5, M.D. Dyar, C. McCammon, M.W. Schaefer (eds.), 327-336, 1996.

Morris, R.V., D.C. Golden, D.W. Ming, T.D. Shelfer, L.C. Jorgensen, J.F. Bell, III, T.G. Graff, S.A. Mertzman, Phyllosilicate-poor palagonitic dust from Mauna Kea Volcano (Hawaii): A mineralogical analogue for magnetic Martian dust?, *Journal of Geophysical Research, 106(E3)*, 5057-5083, 2001.

Newsom, H.E., Hydrothermal alteration of impact melt sheets with implication for Mars, *Icarus, 44*, 207-216, 1980.

Rockwell, B.W., R.N. Clark, C.F. Cunningham, S.J. Sutley, C. Gent, R.R. McDougal, K.E. Livo, and R.F. Kokaly, Mineral mapping and verification in the Marysvale volcanic field, Utah using AVIRIS data, in Summaries of the 9th Annual JPL Airborne Earth Science Workshop, *Jet Propulsion Laboratory Publication 00-18*, 407- 418, 2000.

Reyes, A.G., Petrology of Philippine geothermal systems and the applicaton of alteration mineralogy to their assessment, *Journal of Volcanology and Geothermal Research, 43*, 279-309, 1990.

Simon, J.H., The combined use of multispectral remotely sensed data from the short wave infrared (SWIR) and thermal infrared (TIR) for lithological mapping and mineral exploration, *Fifth Australasian Remote Sensing Conference,* Perth, Western Australia, *1*, 371-380, 1990.

Singer, R.B., Spectral evidence for the mineralogy of high-albedo soils and dust on Mars, *Journal of Geophysical Research, 87*, 1,159-10168, 1982.

Singer, R.B., T.B. McCord, R.N. Clark, J.B. Adams, and R.L. Huguenin, Mars surface composition from reflectance spectroscopy: A summary, *Journal of Geophysical Research, 84*, 8415-8425, 1979.

Smailbegovic, A., J.V. Taranik, W.M. Calvin, Preliminary results of hydrothermal alteration assemblage classification in Aurora and Bodie Mining Districts, Nevada and California, with airborne hyperspectral data, Proceedings of the Tenth JPL Airborne Earth Science Workshop, *Jet Propulsion Laboratory Publication 02-1*, 367-374, 2001.

Swayze, G.A., R.N. Clark, S. Sutley, and A.J. Gallagher, Ground-truthing AVIRIS mineral mapping at Cuprite, Nevada, Summaries of the Third Annual JPL Airborne Geosciences Workshop, Volume 1: AVIRIS Workshop, *Jet Propulsion Laboratory Publication 92-14*, *1*, 47-49, 1992.

Swayze, G.A., The hydrothermal and structural history of the Cuprite Mining District, southwestern Nevada: an integrated geological and geophysical approach, Ph. D. Dissertation, University of Colorado Boulder, 399 pp., 1997.

Ugolini, F.C., Hydrothermal origin of the clays from the upper slopes of Mauna Kea, Hawaii, *Clays and Clay Minerals, 22*, 189-194, 1974.

Vaughan, R.G., W.M. Calvin, J.V. Taranik, Anaylsis of sub-pixel mixing in high-altitude AVIRIS data over Virginia City, Nevada, using systematic field-based observations, Proceedings of the Tenth JPL Airborne Earth Science Workshop*, Jet Propulsion Laboratory Publication 02-1*, 421-426, 2001.

Walter, M.R., D.J. De Marais, Preservation of biological information in thermal spring deposits: developing a strategy for the search for fossil life on Mars, *Icarus, 101*, 129-143, 1993.

Wade, M.L., D.G. Agresti, T.J. Wdowiak, L.P. Armendarez, A Mossbauer investigation of iron-rich terrestrial hydrothermal vent systems: Lessons for Mars exploration, *Journal of Geophysical Research, 104(E4)*, 8489-8507, 1999.

Wolfe, E.W., J. Morris, Geologic Map of the Island of Hawaii, *Miscellaneous Investigation Series Map I-2524-A*, U.S. Geological Survey, 18 pp., 1996.

Wolfe, E.W., W.S. Wise, G.B. Dalrymple, The geology and petrology of Mauna Kea Volcano, Hawaii – A study of postshield volcanism, *U.S. Geological Survey Professional Paper 1557*, 129 pp., 1997.